https://doi.org/10.1016/j.jsv.2015.04.022

Sub-chamber optimization for silencer design

Xiang Yu,[1)] Yuhui Tong,[2)] Jie Pan,[2)] and Li Cheng[1)]

1) Department of Mechanical Engineering, Hong Kong Polytechnic University, Hung Hom, Kowloon, Hong Kong SAR

2) School of Mechanical and Chemical Engineering, University of Western Australia, Crawley, Australia

Abstract

This study proposes sub-chamber optimization for the design of a silencer. A theoretical basis is presented for a description of the overall transmission loss (TL) of the silencer, using the TLs of each of the cascade-connected multiple sub-chambers and the interactions between them. Three typical sub-chamber configurations are considered, representing the effects of varying geometrical parameters, adding internal partitions, and introducing perforated liners. The characteristics of the sub-chambers, influences of the parameters, and the limits of design are investigated to provide guidelines for optimization. It is demonstrated that, by connecting sub-chambers with optimized TLs to tackle different frequency regions, a desired broadband attenuation performance can be achieved. The proposed design scheme with sub-chamber optimization greatly reduces the design variables and calculation costs compared with global optimization, thus offering wider scope in silencer design.

Keywords: silencer design; optimization; micro-perforated panel; folded resonator; multi-chamber silencer.

1. Introduction

The attenuation of broadband noise has always been a challenging topic in the acoustical design of engine exhausts, automotive mufflers, and building ventilation. Reactive and dissipative silencers with a simple expansion chamber have been extensively investigated [1–10]. For reactive silencers, Selamet and Ji [1] studied the effect of adding inlet/outlet extensions on the suppression of the pass-bands of the dome-like transmission loss (TL) pattern. The analytical model was later extended to dual-chamber silencers [2], with induced back pressure evaluated using computational fluid dynamics analysis [3]. With the introduction of perforated liners, silencers designed for a desired acoustic performance with low flow-blockage have been investigated [4-6]. For dissipative silencers, porous materials are commonly used for mitigating mid-to-high-frequency noise [7, 8], but have the disadvantages of being flammable, bulky, non-fibreless, and non-durable. More recently, micro-perforated panel (MPP) silencers were proposed to tackle these problems, and they provide good silencing performance comparable to porous materials while having less engineering constraints [9, 10].

In parallel with the aforementioned studies, optimization based on particular silencer configurations has been the focus of many research studies [11–16]. Barbieri and Barbieri [11], for example, combined a finite element method (FEM) and Zoutendijk's feasible direction for optimization of the silencer shape. Chiu and Chang studied the optimal design of multi-chamber silencers with perforated inlet extensions based on a transfer matrix method with a genetic algorithm [12] and simulated

annealing [13]. Lee *et al.* optimized the layout of internal partitions using two-dimensional FEM modeling with a topology algorithm [14], and considered the flow performance as a necessary objective function simultaneously [15]. Lima *et al.* made a comparison of different optimization techniques for reactive silencers [16].

In practice, a compact size, broadband TL, and simple structure are the preferred features in the design of acoustic silencers. Previous studies have indicated that properly designed multi-chamber silencers may fulfill these requirements [2, 12]. However, although it has been shown that their TL performances can be strongly altered with various design configurations, an efficient optimization scheme is still lacking. On one hand, it is difficult to develop such scheme owing to the uncertainty in choosing optimization variables and objective functions, especially for complicated systems with massive design variables and various engineering constraints. On the other hand, the acoustic modeling techniques adopted in previous designs offer limited capability and flexibility for system optimization. The transfer matrix method, for instance, is limited by the plane wave assumption, whereas FEM can incur a heavy computational cost.

In this paper, a new silencer design framework is proposed to tackle these difficulties, by breaking down the traditional “global” optimization of a silencer into “local” optimization of sub-chambers. For an optimal sub-chamber design, Fig. 1 considers three typical configurations as building blocks for silencer design, allowing varying geometries, adding internal partitions, and introducing perforated panel (PP)/MPP liners. The sub-chamber characteristics, parametric influences, and design

limits of each configuration are first investigated to provide guidelines for subsequent optimization. To numerically model the TL of a silencer, both a conventional FEM and a sub-structuring patch transfer function (PTF) approach [17–19] are employed. While the FEM is capable of handling complex layouts, the PTF approach displays great flexibility and low computation cost in performing subsystem optimization [18]. A detailed comparison between the two methods is given in Sec. 2.2.

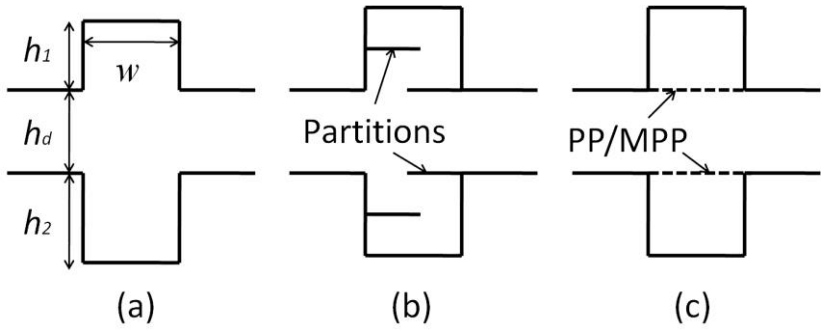

Fig. 1. Three typical sub-chamber configurations representing a) varying geometry, b) internal partitions, and c) internal impedance.

For the coupling between sub-chambers, it has been shown that an array of Helmholtz resonators [20] or cavity resonators [21, 22] can provide a wider TL with each resonator contributing a distinct peak. This has also been validated experimentally through the design of exhaust stack silencers [23]. In this study, the coupling mechanism between sub-chambers is first investigated in Sec. 2.1, serving as a theoretical basis for the proposed design framework. Following the sub-chamber analyses, the feasibility of connecting multiple optimized sub-chambers for broadband attenuation performance is then demonstrated in Sec. 4. The proposed silencer design concept, as well as an efficient optimization tool, demonstrates its potential application in the design of industrial silencers.

2. Formulation of the problem

2.1 Theoretical basis

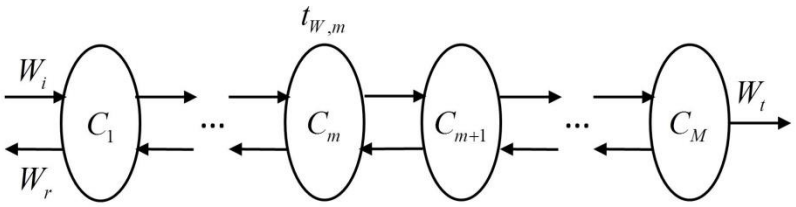

Fig. 2. A system of *M* sub-chambers connected in series.

The theoretical basis of the proposed design scheme is formed by considering a general system comprising *M* acoustic sub-chambers connected in series, as shown in Fig. 2. The input and output of the system are described by the incident, reflected, and transmitted sound powers W_i, W_r, and W_t, respectively. The overall sound power TL of the system is expressed as:

$$\mathrm{TL}_W = 10\log_{10}(W_i / W_t)\,, \tag{1}$$

The sound power transmission coefficient $t_{W,m}$ of the m^{th} sub-chamber is:

$$t_{W,m} = W_{t,m} / W_{i,m}\,, \tag{2}$$

where $W_{i,m}$ and $W_{t,m}$ are, respectively, the incident and transmitted sound powers when the m^{th} sub-chamber is connected with semi-infinite ducts at its two openings. The purpose of this theoretical basis is to establish a link between the overall TL of the system and the TLs of the *M* sub-chambers, which are defined as:

$$\mathrm{TL}_{W,m} = 10\log_{10}\left(1/t_{W,m}\right), \quad \text{for } m = 1,2,...M\,. \tag{3}$$

If the sub-chamber C_2 is directly connected to the outlet of the sub-chamber C_1, then the original output impedance condition (*i.e.*, a semi-infinite duct) for the transmitted sound wave from C_1 is altered by C_2. As a result, the transmitted sound

power from C_1, which is also the incident sound power into C_2, becomes $W_i t_{W,1}(1-\Delta_{1,2})$, where $\Delta_{1,2}$ is a fraction of the reduced sound power in the transmitted sound power from C_1 owing to the change in output impedance. The same analysis can be extended to the coupled sub-chambers shown in Fig. 2 and gives rise to the transmitted sound power from sub-chamber C_M:

$$W_t = W_i \prod_{m=1}^{M} t_{W,m} \prod_{n=1}^{M-1} (1-\Delta_{n,n+1}), \tag{4}$$

leading to the overall TL of the system as:

$$\mathrm{TL}_W = \sum_{m=1}^{M} \mathrm{TL}_{W,m} + 10\log_{10} \prod_{n=1}^{M-1} (1-\Delta_{n,n+1}). \tag{5}$$

To see the influence of $\Delta_{n,n+1}$, two empty cavity resonators with heights of h_{c1} and h_{c2} as sub-chambers C_1 and C_2 are considered in Fig. 3, where their widths w are neglected. In Fig. 3, the uncoupled TL of C_1 with a height of h_{c1} = 0.1 m has one peak at 850 Hz, and the TL of C_2 with a height of h_{c2} = 0.2 m has two peaks at 425 Hz and 1275 Hz, respectively. When the two cavity resonators are connected, the performance is weakened in the overlapping regions between the TLs of the two resonators (around 600 Hz and 1150 Hz), where the deterioration is attributed to the coupling term $\Delta_{1,2}$ ($\Delta_{n,n+1}$) as presented in Eq. (4), but the overall TL of the system exhibits a combined behavior that superposes the TL peaks provided by the two resonators in the non-overlapping frequency range. This indicates that the proposed silencer design formed by cascading different sub-chambers can potentially achieve broadband attenuation performance, as long as the sub-chambers are properly designed and optimized to be effective in different frequency bands.

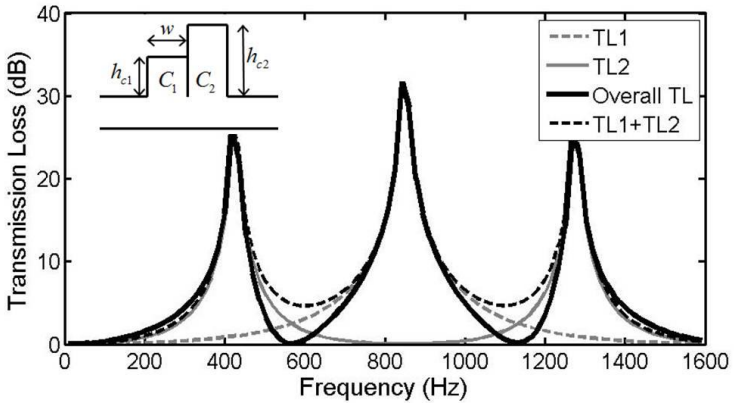

Fig. 3. Coupling effect between two sub-chambers C_1 and C_2.

2.2 Numerical simulation tools

Using the FEM to predict silencer performance has the advantage of being able to cater to complex geometric layouts. Using the commercial FEM software COMOSOL, the acoustic domain is discretized into nodal coordinates. The governing Helmholtz equation assuming time harmonic excitation is described as:

$$\nabla^2 p + k^2 p = 0, \tag{6}$$

where p is the acoustic pressure at each node and k is the wave number.

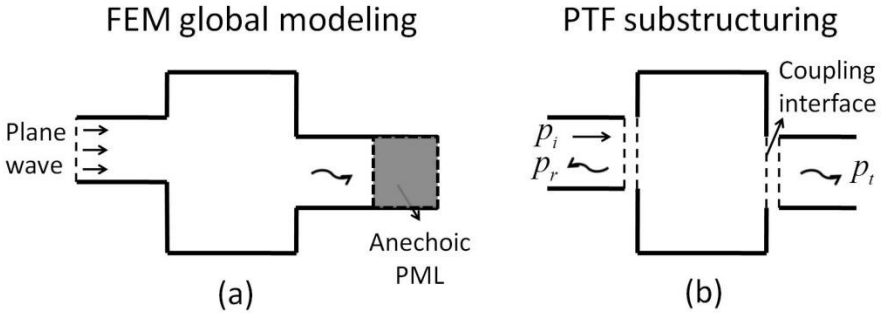

Fig. 4. Comparison of the FEM and PTF sub-structuring approaches.

According to Fig. 4(a), the standard wave equation is solved by applying Neumann boundary conditions on the rigid walls, plane wave excitation at the inlet, and anechoic termination at the outlet. A perfectly matching layer (PML) is

introduced to describe the anechoic condition, which only allows out-going waves with no spurious reflections [24, 25].

Although using the FEM for TL prediction is convenient, it is not well suited for design optimization purposes owing to its high computational cost. In tackling this, a PTF sub-structuring approach [17–19] has been proposed for efficient and flexible optimization of sub-chambers. The global system in Fig. 4(b), being first decoupled into pieces, is assembled by applying transfer functions and continuity conditions at the coupling interfaces. The formulation procedures, particularly for silencer applications, have been detailed in Ref. [18], and thus will not be repeated here.

In comparison to FEM, the PTF approach has a lower computational cost owing to the loosely selected meshing criteria, which is generally $\lambda/6$ for the FEM and $\lambda/2$ for the PTF approach, where λ is the minimum acoustic wavelength of interest [26]. On the other hand, benefiting from the modular nature of the sub-structuring treatment, the PTF approach offers greater flexibility and higher calculation efficiency in performing parametric optimization [18, 19]. Thus, in analyzing the sub-chamber characteristics, both the FEM and PTF approaches are employed for TL predictions, and the presented results in Sec. 3 have been thoroughly validated for accuracy. Meanwhile, for sub-chamber optimization, the PTF approach is implemented owing to its better calculation efficiency.

2.2 Selection of objective functions

Selection of the objective functions is the crucial component in sub-chamber

optimization. The objective function $F(x)$ for maximizing the attenuation performance of a sub-chamber is described as:

$$\max\ F(x) \qquad \text{for}\ \ x=\{x_1,x_2,\cdots\} \tag{7}$$

where x is a vector containing all the design candidates. For each x, $F(x)$ is found by evaluating the averaged TL within a target frequency range Δf, like so [16]:

$$F(x)=\overline{\mathrm{TL}(\Delta f)}=\frac{1}{f_u-f_l}\int_{f_l}^{f_u}W(f)\cdot\mathrm{TL}(f)df=\frac{1}{N}\sum_{n=1}^{N}W_n\cdot\mathrm{TL}_n\,, \tag{8}$$

where f_l and f_u are the lower and upper frequency bounds; n denotes the discrete frequency points in the numerical calculation, N is the total number; and $W(f)$ is a frequency-dependent weighting coefficient, which can be user-defined to correct for human ear perception, actual noise spectrum, *etc*.

By replacing $\mathrm{TL}=10\log_{10}(\tau)^{-1}$, where τ is the power transmission coefficient, $F(x)$ in Eq. (8) can be further expressed as:

$$F(x)=\frac{1}{N}\sum_{n=1}^{N}10\log_{10}\left(\tau_n\right)^{-W_n}=\frac{1}{N}10\log_{10}\left[\prod_{n=1}^{N}\left(\tau_n\right)^{-W_n}\right]. \tag{9}$$

The averaged TL has been commonly adopted as an objective function [11, 14, 16] owing to its easy implementation, especially when the numbers of target frequencies are limited (such as tonal noise). However, the objective function defined in Eq. (9) is difficult to interpret physically. As an alternative, a second objective function $H_2(x)$ is defined as:

$$H_2(x)=\int_{f_l}^{f_u}W(f)\cdot\tau(f)df=\sum_{n=1}^{N}W_n\cdot\tau_n\,. \tag{10}$$

Minimization of this objective function is equivalent to the minimization of frequency-weighted total transmitted power at the outlet, given that the same

incidence condition is applied at all frequencies.

3. Characteristics and optimization of sub-chambers

3.1 Sub-chamber with varying geometrical parameters

The basic configuration of a sub-chamber consists of a rectangular acoustic cavity with two semi-infinite ducts connected on both sides. In Fig. 1(a), the dimensions of an empty sub-chamber are width *w*, heights h_1 and h_2 for the upper and lower side-branch cavities, respectively, and h_d for the inlet and outlet ducts. For cascade applications, sub-chambers with similar outer dimensions are considered. The benchmark case is selected as $w = 0.1$ m, $h_1 = h_d = h_2 = 0.1$ m. In this section, the geometrical effects of varying chamber width *w* and breaking the symmetry by letting $h_1 \neq h_2$ are discussed.

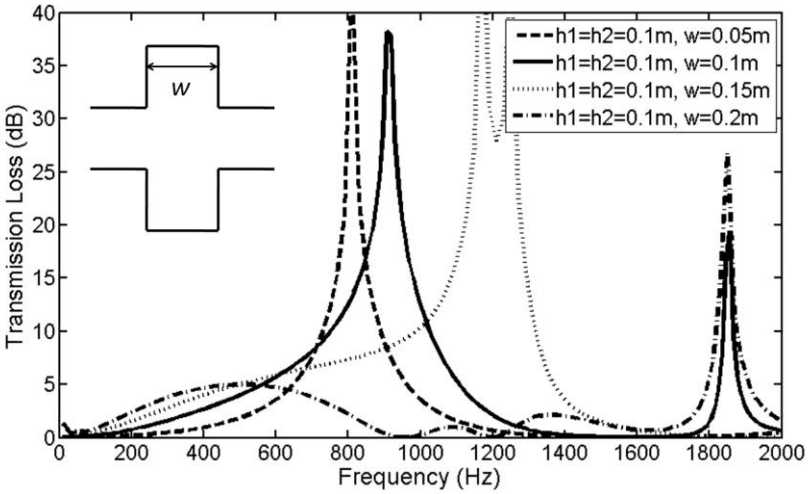

Fig. 5. Effects of varying the chamber width *w*.

In Fig. 5, the TL curves corresponding to the four sub-chambers with *w* varying from 0.05 m to 0.2 m are presented. For the sake of analysis, an acoustic stop-band is defined as TL greater than 10 dB. The benchmark case ($w = 0.1$ m) shows a stop-band

of 750–1050 Hz, with a TL peak located at 917 Hz. At this frequency, the empty chamber acts as a short circuit as a result of impedance mismatch, preventing acoustic power from being transmitted in the downstream direction [5]. Comparing w = 0.05 m and 0.15 m, it can be seen that increasing w shifts the first TL peak toward higher frequencies, while the second peak toward lower frequencies. With w = 0.15 m, the two TL peaks approach each other and combine into a wider stop-band of 950–1350 Hz.

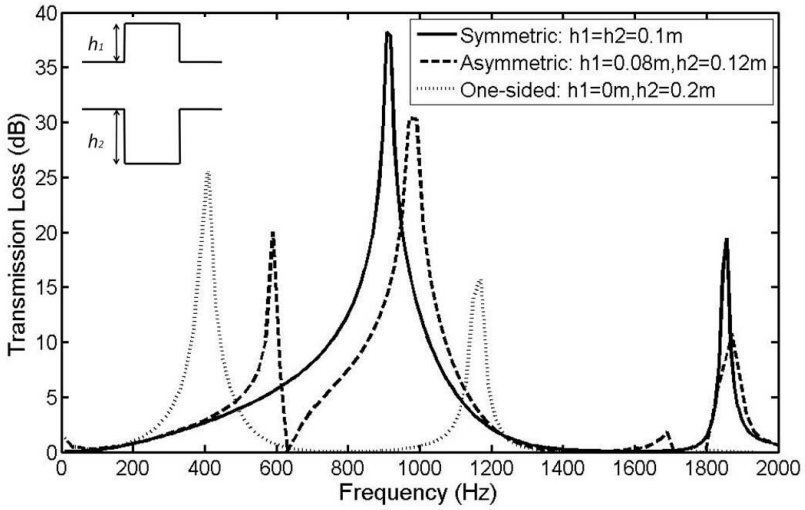

Fig. 6. Effects of the asymmetric duct–cavity system.

With h_1=h_2, the symmetric duct–chamber system induces a single peak of TL below the duct's cut-off frequency. By fixing the total height of h_1+h_2 as 0.2 m, the effect of breaking the symmetry ($h_1 < h_2$) is shown in Fig. 6. By slightly deviating the duct from the center (h_1 = 0.08 m), an extra TL band appears at around 610 Hz, which is generated by the different impedance mismatch characteristics due to the different side-branch heights. This indicates that, by introducing an asymmetric layout, the single TL band of a symmetric chamber can potentially be split in two, with the effective frequency range shifted toward lower frequencies. For the one-sided

chamber (h_1 = 0), the TL band centered at 400 Hz is considered to be the lower limit of such a configuration.

3.2 Sub-chamber with partial internal partition

In Fig. 7, the effect of adding internal partitions to the short sub-chambers is studied. Compared to the benchmark case, a pair of extensions with a length of p = 0.04 m shifts the stop-band toward lower frequencies, to 600–850 Hz, and further increasing p to 0.07 m results in an even lower frequency band. Due to the partial partitions, the characteristic chamber height is effectively lengthened, and thus the TL peak occurs at a lower frequency [18]. In addition, the frequency bandwidth for attenuation of more than 10 dB is decreased as a result of the reduced interaction area. The stop-band with p = 0.04 m is nearly 100 Hz wider than the case with p = 0.07 m (440–600 Hz).

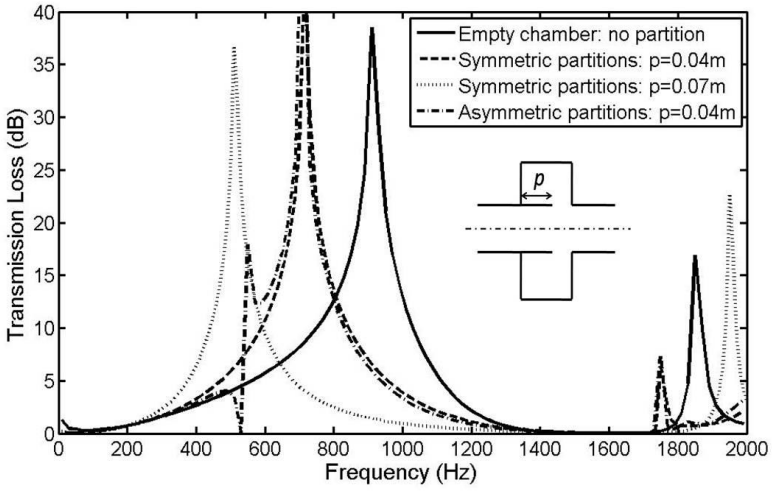

Fig. 7. Effects of partial internal partitions.

In Sec. 3.1, it was shown that an asymmetric system layout can produce an extra TL peak at a frequency below that of the main TL peak. When partitions are

asymmetrically introduced, with one connected to the inlet and the other to the outlet, the TL in Fig. 7 demonstrates that a similar phenomenon occurs, with the lower bound of the stop-band being extended from 600 Hz to 550 Hz. This demonstrates that, in a broader sense, by breaking the system symmetry using various methods, an extra TL peak in the lower frequency range can potentially be activated, and it can be specially designed to tackle strong low-frequency tonal noise.

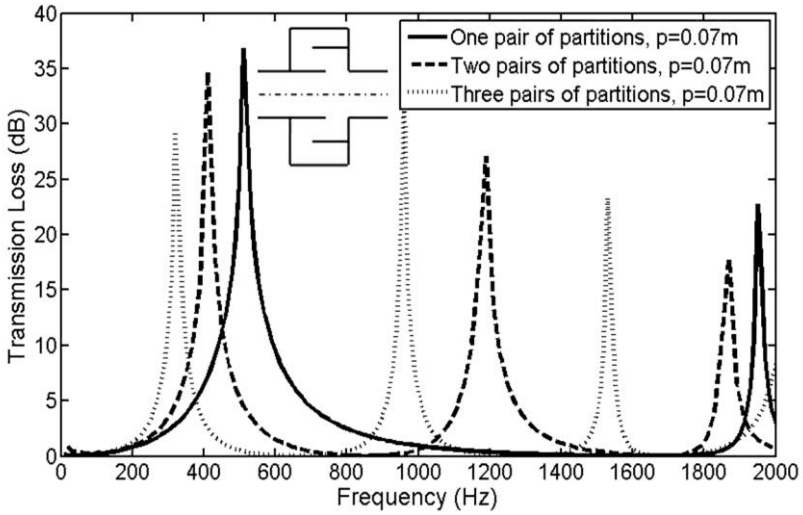

Fig. 8. TLs of sub-chambers with folded partitions.

Additional pairs of partitions folded in the side-branch can be added in order to push the TL band toward even lower frequencies. The configuration in Fig. 8 is typically referred to as a folded resonator [27]. With more pairs of partitions, the tortuous resonator paths further increase the characteristic chamber height, resulting in a lower TL peak at 410 Hz with two folds, and at 320 Hz with three folds. Again, the TL bandwidth is compromised with multiple folds, as a side effect of the reduced aperture size. The stop-band is narrowed to 300–350 Hz with three folds.

3.3 Sub-chamber with a perforated surface

Perforated liners are commonly adopted in silencers in order to reduce back pressure in the presence of air flow. Their influence on the TL is equivalent to the application of a complex impedance to the internal boundary of the silencer. Depending on the diameter of the perforation, a surface with holes greater than 1.5 mm is referred as a perforated surface. If the diameter of the holes is less than 1 mm, then the surface is called an MPP surface. The characteristic impedance of the perforated hole [28, 29] is:

$$Z_p = \sqrt{8\mu\rho_0\omega}\left(1+\frac{t_p}{d_p}\right)+ j\rho_0\omega(t_p+\delta_p), \tag{11}$$

where t_p and d_p are the panel thickness and hole diameter, respectively, and μ, ρ_0, and c_0 are the viscosity of air, density of air, and speed of sound in air, respectively. Finally, δ_p is the term used to characterize the end-correction effect, which can be selected as $\delta_p = 0.25d_p$. The normalized impedance for the perforated surface is then $Z = Z_p / \rho_0 c_0 \sigma$, with σ being the perforation ratio.

For an MPP surface, the impedance of the hole [19] is expressed as:

$$Z_{mp} = \frac{32\mu t_{mp}}{d_{mp}^2}\left[(1+\frac{K^2}{32})^{1/2}+\frac{\sqrt{2}}{32}K\frac{d_{mp}}{t_{mp}}\right]+ j\rho_0\omega t_{mp}\left[1+(1+\frac{K^2}{32})^{-1/2}+0.85\frac{d_{mp}}{t_{mp}}\right], \tag{12}$$

where $K = d_{mp}\sqrt{\rho_0\omega/4\mu}$ and t_{mp} and d_{mp} are the thickness and hole diameter of the MPP.

Figure 9 presents the TLs of sub-chambers with PP/MPP surfaces, showing a strong dependence on hole diameters and perforation ratios. In the simulation, the panel thickness and hole diameter are set to be equal, *i.e.*, $d = t$. Compared with the

stop-band of 750–1050 Hz of the empty chamber, the stop-band with a perforated surface ($d = t = 2$ mm, $\sigma = 4\%$) shifts to 500–730 Hz, and becomes narrower with a lowered TL peak at around 300 Hz with smaller holes close to the MPP range ($d = t = 1.2$ mm, $\sigma = 1\%$). Further reducing the hole size into the MPP range ($d = t = 0.2$ mm) produces a TL with broadband but reduced level of attenuation.

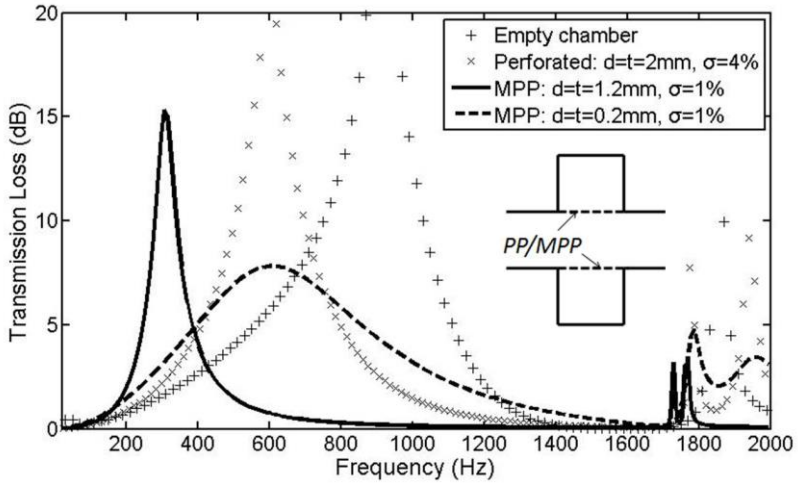

Fig. 9. TLs of PP/MPP surfaces with different hole diameters and perforation ratios.

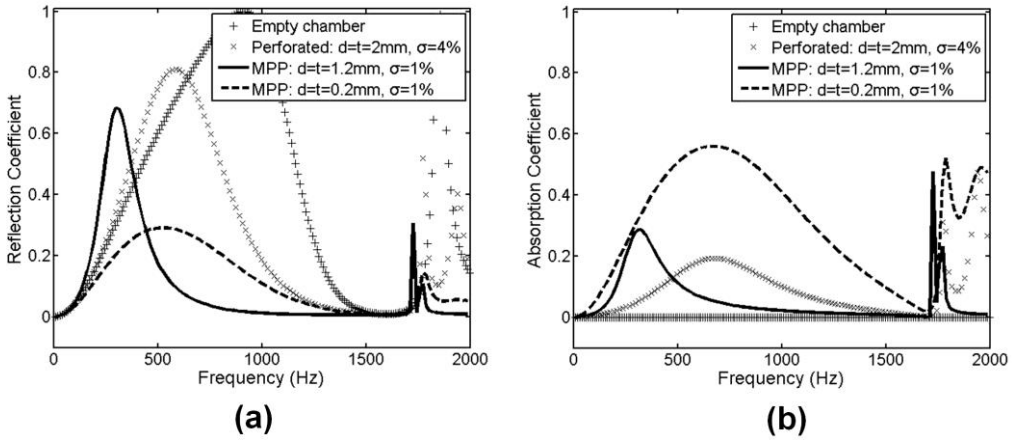

Fig. 10. Comparisons of the (a) reflection coefficients R and (b) absorption coefficients α.

The energy reflection coefficient R and absorption coefficient α, characterizing respectively the reactive and dissipative properties of the sub-chamber, are used to

explain the sound attenuation mechanism involved. The calculations of these using the PTF approach have been detailed in Ref. [19]. By comparing Figs. 10(a) and (b), the *R* curve of the empty chamber shows that a strong TL is purely due to the reactive effect, while α remains at zero. With a perforated liner (d = 2 mm) and MPP (d = 1.2 mm), the reactive property still dominates the TL peak (maximum $R > 0.7$) and the absorption is relatively weak. When using an MPP with smaller holes (d = 0.2 mm), the broadband attenuation is attributed to the greatly enhanced absorptive effect (α > 0.3 in 300–1100 Hz with a maximum of 0.6). In this case, the reactive property has much less influence on TL.

3.4 Sub-chamber optimization

For the optimal design of a silencer using a sub-chamber approach, the characteristics of the TL of the sub-chambers may be summarized as follows:

(1) A symmetric and empty sub-chamber with varying width *w* can be tuned with the location of the TL peak between 800 Hz and 1300 Hz. Using a dimensionless frequency with $f^* = fh_d / c_0$, the corresponding range is between 0.235 and 0.385.

(2) Asymmetric configuration in an empty sub-chamber has the potential to introduce an extra TL peak at lower frequencies.

(3) The center frequency of the stop-band with internal partitions can be shifted lower with a longer partition length or more folded layers. However, with tortuous resonator paths, the attenuation bandwidth is reduced accordingly.

(4) By introducing perforated liners to a sub-chamber, the attenuation mechanism

is seen to exhibit a hybrid effect of both sound reflection and absorption, and different perforation parameters (Fig. 9) show that the stop-band can potentially be designed in the frequency range of 250 Hz to 1100 Hz (or dimensionless frequencies from 0.075 to 0.32).

By incorporating the PTF approach with predefined objective functions, sub-chamber optimization can be performed in a very flexible and efficient way. For illustration purposes, the optimization of an empty sub-chamber with fixed total height while allowing the adjustment of width w and the position of the duct is considered. By fixing h_1+h_2 as 0.2 m and using d to describe the deviation of the duct from the symmetric center, Fig. 11 shows the distribution of the averaged TL defined in Eq. (8) and the total transmitted sound power defined in Eq. (10) as functions of the width w and deviation d. The design domain is constrained as $0.05\,\mathrm{m} \le w \le 0.2\,\mathrm{m}$ and $0 \le d \le 0.1\,\mathrm{m}$. For a target frequency range of 500–1500 Hz (step size 10 Hz), Fig. 11(a) demonstrates the existence of the maximum averaged TL, while Fig. 11(b) shows the minimum total transmitted sound power. In this case, the optimal values of w and d from both figures converge to w = 0.14 m and d = 0 m.

Figure 12 presents the TL as a function of frequency, exhibiting a broadband attenuation with a TL over 5 dB covering the entire intended frequency range. Also presented in Fig. 12 are the configurations for achieving significant TLs in another two frequency ranges, 600–900 Hz and 500–600 Hz. The geometric parameters for these two cases are obtained using both objective functions, $F(x)$ and $H_2(x)$, and converge to w = 0.08 m and d = 0 m, and w = 0.11 m and d = 0.07 m, respectively.

Note that sub-chambers with internal partitions or perforated liners can be optimized within the same regime.

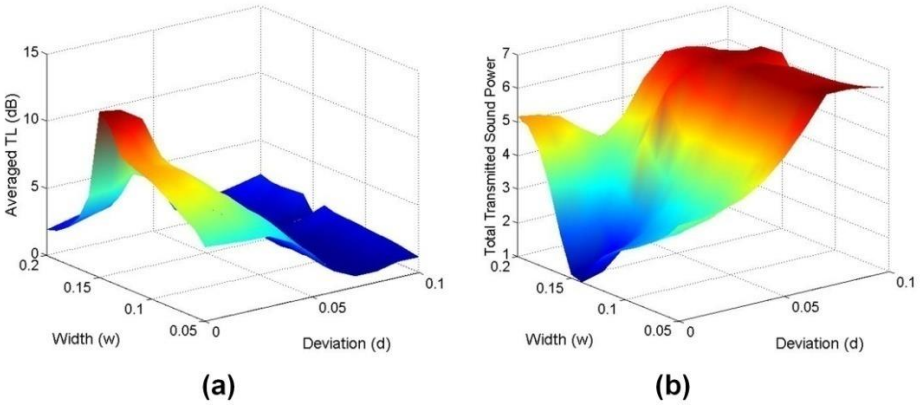

Fig. 11. Distributions of two objective functions: a) the averaged TL and b) the total transmitted sound power (normalized with the minimum value).

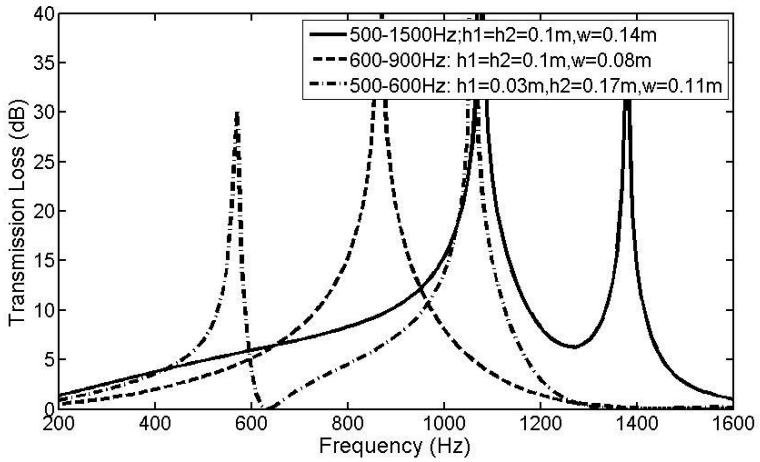

Fig. 12. Optimized TLs for the three target frequency ranges.

4. Combined effect of cascading multiple optimized sub-chambers

As mentioned in Sec. 2.1, a cascade connection of sub-chambers with non-overlapping TLs can potentially lead to a silencer with broadband TL. Based on the understanding of sub-chamber characteristics, two examples of cascade silencers are considered in this section to validate the proposed design scheme. For both

silencers, the heights of the duct and side-branch are fixed at $h_1 = h_d = h_2 = 0.1$ m, and are constructed with four different sub-chambers to tackle different frequency regions. The first example considers a series of reactive sub-chambers, allowing the use of internal partitions and varying chamber widths. The second case uses perforated liners to manipulate the stop-bands provided by each sub-chamber.

The analyses of the TLs of the reactive sub-chambers have shown that a TL of more than 10 dB may cover a frequency range of 250–1400 Hz (dimensionless frequencies ranging roughly from 0.08 to 0.4). Thus, in the following sub-chamber design, four frequency subintervals are used for the design of individual sub-chambers. Their ranges are 300–500 Hz, 500–700 Hz, 700–1000 Hz, and 1000–1400 Hz, respectively. In Fig. 13, the lowest TL band centered at 400 Hz can be easily tackled using two-fold partitions ($p = 0.07$ m). With one pair of partitions ($p = 0.06$ m), the second TL band centered at 600 Hz can also be resolved. For the mid-to-high frequencies, adjusting the width w to 0.08 m and 0.15 m achieves a TL of more than 10 dB in 720–970 Hz and 980–1380 Hz, respectively.

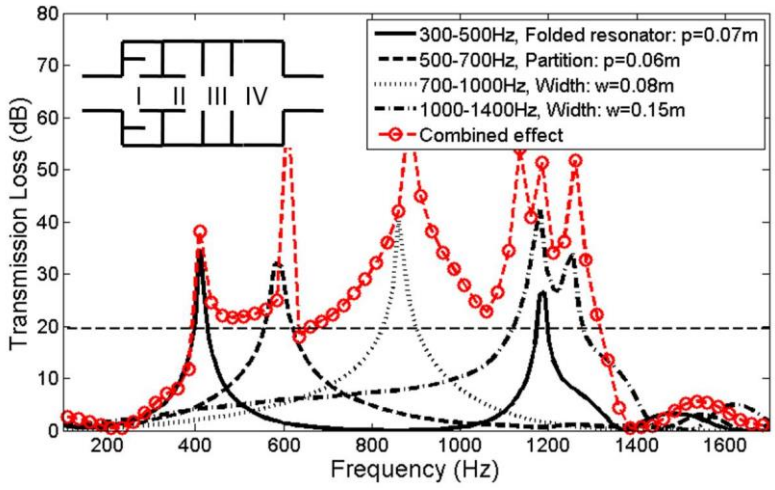

Fig. 13. TLs of broadband reactive silencer realized by cascading four optimized

sub-chambers.

Once the four optimized sub-chambers are connected, a greatly enhanced broadband TL (Fig. 13) is achieved, with a stronger stop-band (TL > 20 dB) ranging from 380 to 1350 Hz. Corresponding to the peak frequencies of the combined TL at 400, 600, 860, and 1120 Hz, respectively, Fig. 14 shows that the sound attenuation is dominated by the reactive effect of each sub-chamber, which demonstrates the local effects of the proposed design. At the resonance frequency of each sub-chamber, the induced strong impedance mismatch allows hardly any sound waves to be transmitted through the silencer.

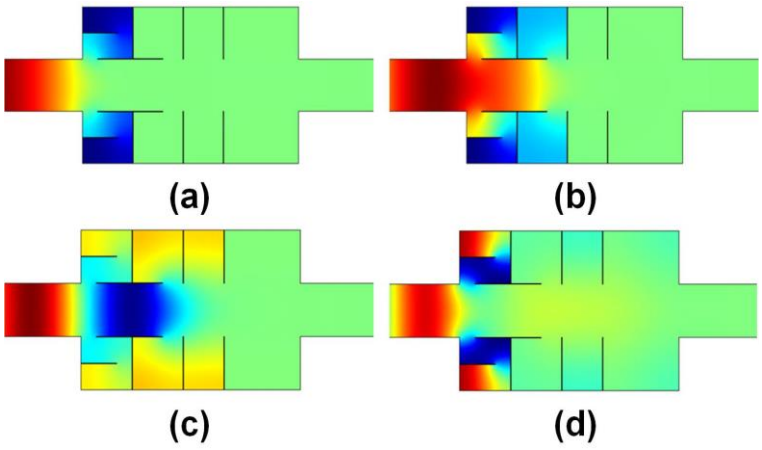

Fig. 14. Visualized pressure fields at the four TL peak frequencies: (a) 400 Hz, (b) 600 Hz, (c) 860 Hz, and (d) 1120 Hz.

By introducing perforated liners, the frequency range of the effective TL band of the silencer can be changed to within 250–1100 Hz. In Fig. 15, a straight-through silencer with perforated surfaces is intended to work over 200–1000 Hz. The thickness of the perforated surface is fixed at t = 1 mm. For 200–400 Hz, optimization shows that a hole of diameter d = 5.9 mm and a perforation ratio of σ = 1% can provide a stop-band of 260–380 Hz. Meanwhile, for 400–600 Hz and 600–800 Hz, the

same hole size but with different perforation ratios (2.5% and 7.5%) can readily provide two stop-bands covering 420–570 Hz and 570–820 Hz. The last chamber is designed to have large hole size and high perforation ratio, which is equivalent to an empty chamber operating at frequencies of 750–1050 Hz. After their connection, the overall TL again exhibits a combined broadband behavior, with a much wider stop-band with a TL of more than 10 dB cover 250–1100 Hz. It is noted that, although the sequence of sub-chambers also exerts an influence on the TL, the acoustic coupling between them is very complex and thus beyond the scope of the present study.

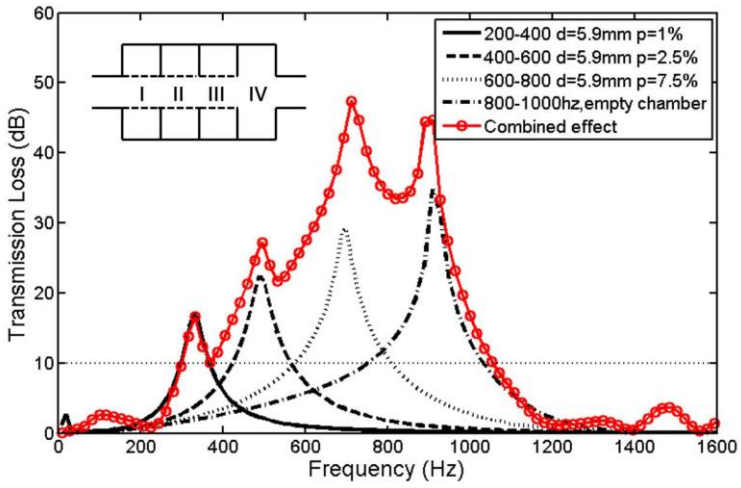

Fig. 15. TLs of broadband multi-chamber silencer found by optimizing the perforated surface.

5. Conclusion

The feasibility of achieving broadband sound attenuation by using silencers with cascade sub-chambers was demonstrated. The coupling mechanism of the sub-chambers was investigated, providing an explanation of the overall broadband

transmission loss (TL) of the silencer. The features of three common types of sub-chambers were then discussed, serving as building blocks for the coupled system.

By varying the geometry of an empty sub-chamber, the peaks and dips of the chamber's TL due to impedance mismatch can be designed at targeted frequencies. A single TL peak can potentially be separated into two peaks with one in a lower frequency range by breaking the system's symmetry. By using sub-chambers with extensions or folded partitions, the peak of the TL may be shifted to the lower frequency and its bandwidth reduced. A sub-chamber with perforated liners was also studied. The perforation parameters can be adjusted to provide the desired reactive and resistive contributions for the required location and bandwidth of the TL.

The TL characteristics of the three types of sub-chambers were summarized to provide design guidelines for the overall TL of a silencer constructed by cascading the sub-chambers. For the optimization of the sub-chamber TL, the patch transfer function (PTF) approach, which provides better calculation efficiency, was adopted, together with two objective functions selected to maximize the averaged TL or minimize the total transmitted power. With an optimized design for each sub-chamber, the overall TL of the cascaded sub-chambers exhibited an excellent broadband attenuation performance. Compared with global optimization of a silencer, optimizing the design of a sub-chamber requires less design variables and therefore less computational cost. Therefore, the proposed sub-chamber optimization technique is better suited to the practical design of industrial silencers.

Acknowledgements

The authors wish to acknowledge the support from the Research Grants Council of the Hong Kong Special Administrative Region, China (PolyU 5103/13E and 152026/14E) and the Australian Research Council, Australia. The first author is grateful to the Research Office of HK PolyU for providing financial support for his exchange program at UWA. The second author would like to thank the Chinese Scholarship Council for its financial support.

REFERENCES

1. A. Selamet, Z. L. Ji, Acoustic attenuation performance of circular expansion chambers with extended inlet/outlet, *Journal of Sound and Vibration* **223** (1999) 197–212.

2. A. Selamet, F. D. Denia, A. J. Besa, Acoustic behavior of circular dual-chamber mufflers, *Journal of Sound and Vibration* **265** (2003) 967–985.

3. J. M. Middelberg, T. J. Baber, S. S. Leong, K. P. Byrne, E. Leonardi, Computational fluid dynamics analysis of the acoustic performance of various simple expansion chamber mufflers, *Proceedings of Acoustics* (2004) 123–127.

4. A. J. Torregrosa, A. Broatch, R. Payri, F. Gonzalez, Numerical estimation of end corrections in extended-duct and perforated-duct mufflers, *Journal of Vibration and Acoustics* **305** (1999) 302–308.

5. M. L. Munjal, *Acoustics of ducts and mufflers*, John Wiley & Sons, 2014.

6. I. J. Lee, Acoustic characteristics of perforated dissipative and hybrid silencers, Doctoral dissertation, The Ohio State University, 2005.

7. R. Kirby, Simplified techniques for predicting the transmission loss of a circular dissipative silencer, *Journal of Sound and Vibration* **243** (2001) 403–426.

8. A. Selamet, M. B. Xu, I. J. Lee, N. T. Huff, Analytical approach for sound attenuation in perforated dissipative silencers, *Journal of the Acoustical Society of America* **115** (2004), 2091–2099.

9. X. N. Wang, Y. S. Choy, L. Cheng, Hybrid noise control in a duct using a light micro-perforated plate, *Journal of the Acoustical Society of America* **132** (2012) 3778–3787.

10. S. Allam, M. Åbom, A new type of muffler based on microperforated tubes, *Journal of Vibration and Acoustics* **133** (2011) 031005-1–031005-9.

11. R. Barbieri, N. Barbieri, Finite element acoustic simulation based shape optimization of a muffler, *Applied Acoustics* **67** (2006) 346–357

12. M. C. Chiu, Y. C. Chang, Numerical studies on venting system with multi-chamber perforated mufflers by GA optimization. *Applied Acoustics* **69** (2008) 1017–1037.

13. M. C. Chiu, Y. C. Chang, Shape optimization of multi-chamber cross-flow mufflers by SA optimization, *Journal of Sound and Vibration* **312** (2008) 526–550.

14. J. W. Lee, Y. Y. Kim, Topology optimization of muffler internal partitions for improving acoustical attenuation performance. *International journal for numerical methods in engineering* **80** (2009) 455–477.

15. J. W. Lee, G. W. Jang, Topology design of reactive mufflers for enhancing their acoustic attenuation performance and flow characteristics simultaneously. *International Journal for Numerical Methods in Engineering* **91** (2012) 552–570.

16. K. F. De Lima, A. Lenzi, R. Barbieri, The study of reactive silencers by shape and parametric optimization techniques, *Applied Acoustics* **72** (2011) 142–150.

17. X. Yu, L. Cheng, J. L. Guyader, Modeling vibroacoustic systems involving cascade open cavities and micro-perforated panels, *Journal of the Acoustical Society of America* **136** (2014) 659–670.

18. X. Yu, L. Cheng, Duct noise attenuation using reactive silencer with various internal configurations, *Journal of Sound and Vibration* (2014) (In press)

19. X. Yu, L. Cheng, Y. H. Tong, J. Pan, Sound attenuation using duct silencers with micro-perforated panel absorbers, *Inter-noise 2014*, Melbourne, Australia (2014)

20. S. H. Kim, Y. H. Kim, Silencer design by using array resonators for low-frequency band noise reduction, *Journal of the Acoustical Society of America* **118** (2005) 2332–2338.

21. S. K. Tang, Narrow sidebranch arrays for low frequency duct noise control, *Journal of the Acoustical Society of America* **135** (2012) 3086–3097.

22. S. K. Tang, H. M. Yu, K. C. Ho, Effect of low mach number flow on the sound transmission loss of sidebranch array, *The 21st International Congress on Sound and Vibration*, Beijing, China (2014)

23. C. Q. Howard, B. S. Cazzolato, C. H. Hansen, Exhaust stack silencer design using finite element analysis, *Noise Control Engineering Journal* **48** (2000) 113–120.

24. T. Graf, J. Pan, Determination of the complex acoustic scattering matrix of a right-angled duct, *Journal of the Acoustical Society of America* **134** (2013) 292–299.

25. S. Hein, W. Koch, L. Nannen, Trapped modes and Fano resonances in two-dimensional acoustical duct–cavity systems, *Journal of Fluid Mechanics* **692** (2012) 257–287.

26. J. D. Chazot, J. L. Guyader, Prediction of transmission loss of double panels with a patch-mobility method, *Journal of the Acoustical Society of America* **121** (2007) 267–278.

27. R. Glav, P. L. Regaud, M. Åbom, Study of a folded resonator including the effects of higher order modes, *Journal of Sound and Vibration* **273** (2003) 777–792.

28. A. B. Bauer, Impedance theory and measurements on porous acoustic liners, *Journal of Aircraft* **14** (1977) 720–728.

29. S. H. Lee, J. G. Ih, Empirical model of the acoustic impedance of a circular orifice in grazing mean flow, *Journal of the Acoustical Society of America* **114** (2013) 98–112.

Figure Captions

Fig. 1. Three typical sub-chamber configurations representing a) varying geometry, b) internal partitions, and c) internal impedance.

Fig. 2. A system of M sub-chambers connected in series.

Fig. 3. Coupling effect between two sub-chambers C_1 and C_2.

Fig. 4. Comparison of the FEM and PTF sub-structuring approaches.

Fig. 5. Effects of varying the chamber width w.

Fig. 6. Effects of the asymmetric duct–cavity system.

Fig. 7. Effects of partial internal partitions.

Fig. 8. TLs of sub-chambers with folded partitions.

Fig. 9. TLs of PP/MPP surfaces with different hole diameters and perforation ratios.

Fig. 10. Comparisons of the (a) reflection coefficients R and (b) absorption coefficients α.

Fig. 11. Distributions of two objective functions: a) the averaged TL and b) the total transmitted sound power (normalized with the minimum value).

Fig. 12. Optimized TLs for the three target frequency ranges.

Fig. 13. TLs of broadband reactive silencer realized by cascading four optimized sub-chambers.

Fig. 14. Visualized pressure fields at the four TL peak frequencies: (a) 400 Hz, (b) 600 Hz, (c) 860 Hz, and (d) 1120 Hz.

Fig. 15. TLs of broadband multi-chamber silencer found by optimizing the perforated surface.